# THIN FILM HEAT TRANSFER DATA REDUCTION BY MEANS OF SOME NUMERICAL TECHNIQUES

Lorenzo Battisti and Enrico Bertolazzi

*Dip. Ingegneria Meccanica e Strutturale, Università di Trento,*
*via Mesiano 77, I – 38050 Trento, Italy*
*Fax : +39 0461 882599  Voice : +39 0461 882660*

**Abstract**

A thin-film sensor operated in transient mode in principle enables very accurate surface temperature measurements to be obtained partly because the gauge is non-intrusive and partly because the high frequency of its response. The major drawback for its popular use is the complexity of data reduction procedure which involves the solution of the heat conduction in solids. Among different techniques available, numerical discretization is gaining in importance for several applications basically because of their flexibility in treating boundary conditions and the low computational cost compared to other methods. After a brief analysis of the heat transfer evaluation criteria and the description of the sensor, a survey of the existing digital data processing technique is discussed in the first part of this paper, and some estimate of the accuracy is presented. The general case of multi-layered geometries of the sensor is analyzed and synthetic expressions for the single and double layer features are given. Among the traditional methods, emphasis was placed on 1-D Finite Elements discretization, and a code has been developed to handle general heat transfer data reduction with arbitrary temperature or heat flux boundary conditions. Temperature dependent physical properties are also implemented. Validation of such a code has been performed by mens known test functions. Finally several experimental signals having different characteristics have been processed and the solution of the various methods compared and discussed.

*Key words:* Thin film, heat transfer, surface temperature measurements, Laplace Transform, Finite Elements.

## 1 Nomenclature

| | |
|---|---|
| $\rho(z)$ | one dimensional mass density of the slab; $[kg/m^3]$ |
| $c(z)$ | heat capacity of the slab; $[J/kg \cdot K]$ |
| $\kappa(z)$ | heat conduction of the slab; $[W/m \cdot K]$ |
| $\alpha$ | $= \kappa/\rho c$ thermal diffusivity; $[m^2/s]$ |
| $\delta$ | metal film thickness; $[m]$ |
| $\ell$ | total size of the slab; $[m]$ |
| $\dot{q}_s(t)$ | impinging convective heat flux rate; $[W/m^2]$ |
| $\dot{q}_b(t)$ | back face convective heat flux rate; $[W/m^2]$ |
| $u(t)$ | internal density energy stored into the slab; $[J/m^2]$ |
| $\Theta(t, z)$ | temperature distribution of the slab; $[K]$ |
| $\Theta^s(t)$ | measured top surface temperature of the slab; $[K]$ |
| $\Theta^\infty(t)$ | free stream temperature; $[K]$ |
| $\mathrm{F}_c\,(t)$ | Fresnel cosine function; |
| $\mathrm{F}_s\,(t)$ | Fresnel sine function; |
| DAS | Digital Analog System; |
| ODE | Ordinary Differential Equation; |
| PDE | Partial Differential Equation. |

## 2 Introduction

The evaluation of the heat flux rate impinging on a surface is an important task in engineering problems. One of the most adopted approaches for its evaluation is the indirect approach. It prescribes the measurement of some physical quantities such

as the body surface temperature. The heat flux rate is deduced by the solution of some auxiliary equations.

Although this method does not give any information for the comprehension of the transport phenomena, yet, it has been, over the years, the most widely adopted because it requires a limited number of measurements and involves only the solution of the diffusion equation in a body.

Short duration facilities have been preferred to the stationary ones for indirect methods because of the competitive running costs and the good measurement accuracy achievable. In fact the models have not to be cooled (or heated) in order to establish the temperature gradient from which the heat transfer is deduced. Consequently test durations are shorter and the initial conditions are quickly restored. In net heat flux evaluations, conductive heat losses are not crucial. The measurement technique involves the measurement of the surface temperature history of a model exposed to a gas flow (supersonic or subsonic) on the basis of an appropriate heat conduction model.

Despite of the complexity of the data reduction procedures, a variety of techniques has been implemented and refined according to the type of test and sensor being used. A basic reference text describing measurement principles and data reduction techniques can be found in the work of Schultz and Jones [24].

One of the most common fast response sensors for short duration tests is the thin film resistance thermometer. A large body of literature is available on the thin film heat transfer gauge. Diller [9] gives an excellent survey of the related measurement techniques. Here just a brief part of the progress in data reduction procedures will be drawn. Details of the sensors will be given in section 3.

The thin film surface temperature sensor has originally appeared in the early 1950s for heat transfer measurements in shock tubes. This facility can be operated to simulate either supersonic or subsonic environment depending on the location of the throat with respect to the working section. A very wide range of the temperatures, from $500K$ to $2000K$ can be achieved. Depending on the hardware, typical test durations can range from $3ms$ (the Oxford shock tunnel) to a few seconds. A review is given in Vidal [26], Pope and Goin [23], Lukasiewicz [17]. Direct solution

of the 1-D diffusion equation was initially performed by means of the electrical analogy [20]. In the 1960's some numerical integration techniques for the solution of the heat diffusion equation were proposed. All these schemes were based on an approximate solution of the associate Laplace transform. The most popular one, proposed by Cook and Felderman [8] will be addressed in section 5.

Starting from 1975 M.G. Dunn and its group in Calspan applied the thin film in order to measure heat flux distribution for gas turbine components. Vane row and full stage rotating turbine data have been the subject of several papers by Dunn and Hause [13], Dunn, Martin, and Stanek [14], Dunn [12]. The progress in the computational media has made possible to improve the numerical techniques. The computer implementation of Fourier and Laplace transforms permitted to optimize the frequency response and the accuracy of the time-resolved results.

Wide experience on the so called "double layer'/' thin films has been developed from the group working at the Oxford University [21], and Ainsworth, Allen, Davies, and et al. [1].

The attempt to measure the mean heat transfer rate on real gas turbine components has lead to films instrumented on the flexible electrically insulator substrate (kapton® or upilex®) to extend the use of this measurement technique to rotating test rig components where flow durations are of the order of a few seconds.

Analog signal analysis has been used for data reduction on films built also with vitreous enamel substrate considering that the high frequency heat conduction in the insulating layer can be considered, for short times, as semi-infinite. An additional digital processing is moreover needed for the low frequency signal of the substrate layer Ainsworth *et al.* [1], Doorly and Oldfield [11], Doorly [10], Guo, Spencer, Lock, and Jones [16].

At the von Karman Institute single layer thin films using mainly macor® as substrate have now been used for many years on the Mach 6 H-3 blow down wind tunnel, the long shot intermittent wind tunnel, and the CT 3 light piston facility. Recently a double layer thin film with kapton® as substrate has been tested on low speed tunnels simulating flow conditions in gas turbine blade internal cooling channels. Main results can be found in Consigny and Richard [7], Camci and Arts [6], Battisti

and Arts [3], Pelle and Arts [22], Vermeulen and Simeonides [25] and Marquet and Charbonnier [19].

The extension of the use of thin films to the evaluation of the fluctuating component of the heat transfer and the necessity to account for variable properties of the substrate has lead to a progressive phase out of the analogue technique.

Numerical techniques seemed to have the potential to provide a powerful solving tool. Up to now, some data processing analysis was principally based on transforms such as Laplace or Fourier.

Both analog signal analysis and numerical transform based solution methods do present some limitations which basically are:

- $(i)$ the analog hardware necessitates a bandwidth depending on the sampling rate. A high sampling rate needs an hardware with very high bandwidth.
- $(ii)$ the impossibility to model variable thermal properties of the substrate(s) with the temperature;
- $(iii)$ operations are bounded to semi-infinite slab assumption;
- $(iv)$ the solution is computationally expensive with two substrate slabs and, when the number of substrate slabs excesses two, it becomes mathematically difficult to handle.

The best implementation of the aforementioned numerical techniques has a complexity growing at least with $\mathcal{O}(n_s \log n_s)$ where $n_s$ is the number of samples.

In the first part of the paper some data reduction techniques are reviewed. In the second part a general approach based on Finite Elements is presented for fast and efficient heat flux computation. In Figure 1 it is shown the physical model adopted; the free stream temperature $\Theta^{\infty}(t)$ and the surface temperature $\Theta^{s}(t)$ are known from standard measurement devices while the impinging heat flux rate $\dot{q}_s(t)$ can be inferred by an appropriate differential model of the substrate.

It is worth to remind that temperature $\Theta^{s}(t)$ is the result of a thermal balance among different heat fluxes. The principal ones are the convective heat flux $\dot{q}_s(t)$, the radiative heat flux, the conductive heat flux and the heat flux due to electrical heat generation of measurements apparatus. In the following discussion, it is assumed

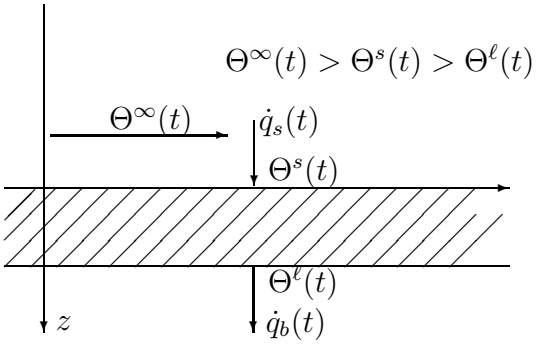


Fig. 1.

that the temperature $\Theta^s(t)$ depends only on the convective and the conductive heat flux, neglecting the other sources.

For a proper reconstruction of the signal an appropriate sampling rate must be assured. The limitation in the capacity of the acquisition system sets the maximal test duration. However the sampled data is usually huge and the postprocessing is very time consuming if a transform based data reduction system is used. The Finite Element based data reduction, proposed in this paper, is very fast, more flexible but, depending on the sampling rate, requires the correct setting of the mesh.

The proposed numerical scheme has been validated by using known exact solutions of particular test cases, and by comparison with the classical numerical techniques.

A processing of three real signals is given. The heat flux rate is deduced from surface temperature histories sampled on models running on different facilities. The first signal has been obtained from tests performed with a double layer thin film made by the University of Trento in low enthalpy and low speed test (about $\dot{q} = 1000 W/m^2$, Re $= 30000$, Ma $= 0.02$) Battisti and Schmeer [4]. The second one is a signal sampled in the von Karman Institute CT2 tunnel at Mach number around $0.7$ (single layer thin film). The last case has been obtained from a compression ramp in the H3 Mach 6 wind tunnel of the von Karman Institute (single layer thin film) Marquet and Charbonnier [19].

The performance of the different solution schemes have been compared and commented.

## 3 The thin film surface temperature sensor

There are many different techniques currently available for surface temperature measurements. The present paper is focused on the thin film resistance thermometer.

Basically the thin film gauge consists in a very thin conducting metal (platinum or nickel) deposited on a homogeneous or disomogeneous substrate. As the metal acts as temperature sensor, the substrate serves as mechanical support and as thermal heat sink. The most popular features of such devices are the single and the double layer thin films. The thermal behavior of these two kinds of sensors will be analyzed forward. In the first type (see Fig. 2a) the metal layer is fired or de-

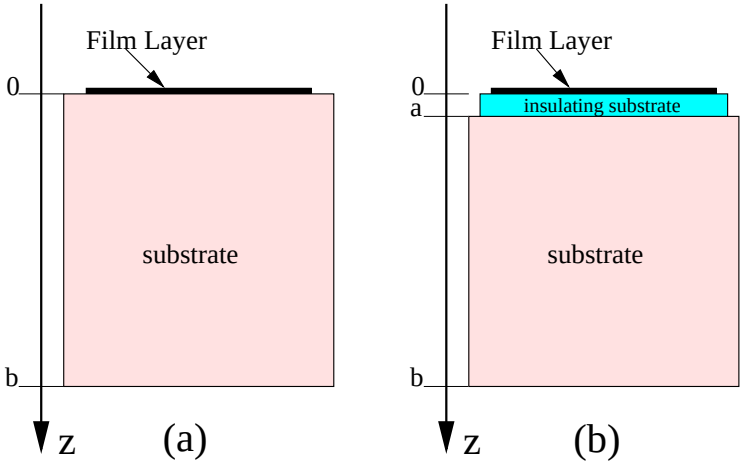


Fig. 2.

posited on a substrate made of quartz, pyrex® or macor®. In particular the use of macor® (machinable ceramic) enables the desired shape model to be built without surface discontinuities. This makes the gauge particularly suitable for aerodynamic applications where the integrity of the boundary layer has to be preserved.

Such solutions are suitable for stationary components due to the limited deformation of the substrate. The double layer thin film (see Fig. 2b) has been developed for measurement on rotating components. A thin layer insulates electrically the metal film from the (metal) support. Either vitreous enamel is applied as insulating coating or a plastic layer (kapton® or upilex®) is adhesively bounded to the substrate.

A known constant current is passed through the gauge and the voltage drop across

the film is directly related to the temperature of the gauge. When subjected to a change in the temperature field, the film acts as a thermometer and under some assumptions it shows the temperature evolution of the substrate surface. Since the typical thickness $\delta$ of the film ranges from $10^{-6}m$ to $10^{-8}m$ and this dimension is $10^5$ times smaller than its typical length or width, the lateral conduction can be neglected. Therefore the one-dimensional heat conduction can generally be applied.

The characteristic time $\tau = \delta^2/\alpha$ of the film is dramatically small compared to the inner substrate one.

For the typical thickness given above, characteristic times range from $1.6 \cdot 10^{-3}\mu s$ (platinum painted on macor®) to $2 \cdot 10^{-4}s$ (nickel over kapton®). For a step function in surface heat transfer rate, the approximate solution for the relative error in the heat transfer rate computation ($\epsilon = (q - \dot{q}_s)/\dot{q}_s$), as shown in [24] can be estimated as follows for large $t$ compared to $\tau$:

$$\epsilon = \frac{1}{\sqrt{t}} \frac{\sqrt{\tau}}{\sqrt{\pi}} \frac{\sqrt{(\rho c \kappa)_1}}{\sqrt{(\rho c \kappa)_2}}, \tag{1}$$

where the index $1$ refers to the sensor and $2$ to the supporting substrate. Relation (1) shows that the error due the neglect of the sensor presence drops as time increases. When a maximum allowable error is given, relation (1) introduces a critical time in the initial part of the experiment. For $\epsilon \approx 10^{-2}$, this minimal duration takes the values of about $400\mu s$ for a typical double layer sensor to about $100\mu s$ for a single layer. The reciprocal of this critical time represents the critical frequency over over which the phenomenon is not accurately reconstructed.

The effect of the finite thickness of the sensible layer on the insulating substrate is thus to cause the actual surface temperature to lag the “real” one.

For general applications, other than shock tubes the presence of the film layer can be neglected if the experiment design is carefully set.

Whatever model being used, the heat flux rate can be generally evaluated from considerations about the transient thermal conduction in an inhomogeneous multi-slab substrate.

The governing equations for a general multi-slab substrate are addressed in the next

section.

## 4 Governing equations

The 1-D diffusion equations for the temperature distribution of a $m-$layer slab having a total size $\ell$ (see Figure 3), can be modeled by the following $m$ partial differential equations of parabolic type:

$$\frac{\partial}{\partial t}\left(\rho_i c_i \Theta\right) = \frac{\partial}{\partial z}\left(\kappa_i \frac{\partial \Theta}{\partial z}\right), \quad \begin{array}{c} t > 0, \\ z_{i-1} < z < z_i \end{array} \tag{2}$$

for $i = 1, 2, \ldots, m$, where $\Theta \equiv \Theta(t, z)$ is a continuous piecewise $C^1$ function, $\rho_i \equiv \rho_i(\Theta)$, $c_i \equiv c_i(\Theta)$ and $z_i$ are the boundaries of the layers with $z_0 = 0$ and $z_m = \ell$. Equations (2) are coupled with the following $m - 1$ interface conditions:

$$\lim_{z \mapsto z_i^-} \kappa_i \left(\Theta(t, z)\right) \frac{\partial \Theta(t, z)}{\partial z} = \lim_{z \mapsto z_i^+} \kappa_{i+1} \left(\Theta(t, z)\right) \frac{\partial \Theta(t, z)}{\partial z},$$

for $t > 0$ and $i = 1, 2, \ldots, m - 1$. The *impinging convective heat flux rate* $\dot{q}_s(t)$

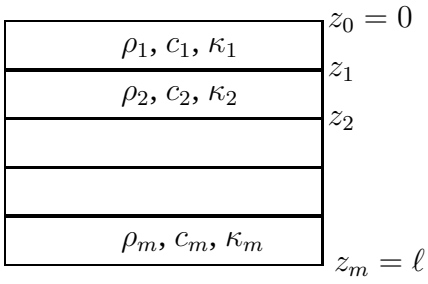


Fig. 3.

and the *backface convective heat flux rate* $\dot{q}_b(t)$ are defined as follows:

$$\dot{q}_s(t) = -\kappa_1(\Theta(t, 0)) \left.\frac{\partial \Theta(t, z)}{\partial z}\right|_{z=0}, \tag{3}$$

$$\dot{q}_b(t) = -\kappa_m(\Theta(t, \ell)) \left.\frac{\partial \Theta(t, z)}{\partial z}\right|_{z=\ell} \tag{4}$$

The differential equation (2) is closed by the initial temperature distribution $\Theta(0, z) = \Theta^{init}(z)$, for $0 \leq z \leq \ell$, and boundary conditions. At the surface, i.e. $z = 0$ if $\Theta^s(t)$ is given:

$$\Theta(t, 0) = \Theta^s(t), \tag{5}$$

Analogously on the back surface, i.e. $z = \ell$ equation (4) is given. As a temperature signal $\Theta^s(t)$ is assigned, it is possible to solve the differential equation (2) with surface boundary condition (5) to obtain the body temperature distribution $\Theta(t, z)$ and by (3) heat rate $\dot{q}_s(t)$ is thus evaluated. Only in a few simple cases $\Theta(t, z)$ can be computed exactly, and generally it must be approximated by means of numerical techniques.

## 5 One layer slab

In this case the slab has everywhere constant physical properties so that the indices in $\rho_1$, $c_1$ and $\kappa_1$ are omitted. If the test duration is short enough and/or the thickness of the slab is properly chosen, the finite slab can be modeled by a semi-infinite one. Moreover, if the temperature inside the slab does not increase too much, the following approximations hold:

$$\rho(\Theta) \equiv \rho, \quad c(\Theta) \equiv c, \quad \kappa(\Theta) \equiv \kappa, \tag{6}$$

i.e. their values are assumed constant and evaluated at the initial temperature. This is the case when the diffusivity of the layer is sufficiently low or the impinging heat flux is moderate.

The one dimensional semi-infinite slab is modelled by equation (2) with $\ell = \infty$ and $m = 1$. The slab is assumed to be in thermal equilibrium at time $t = 0$, so that (without loss of generality) we assume $\Theta(0, z) = 0$ for all $z \geq 0$. With assumption (6) the equation (2) can be easily solved by means of the Laplace transform expressing $\dot{q}_s(t)$ in function of $\Theta(t, 0)$ or vice versa by the following equations:

$$\dot{q}_s(t) = \frac{\sqrt{\rho c \kappa}}{\sqrt{\pi}} \int_0^t \frac{\frac{\partial \Theta(t,0)}{\partial t}\Big|_{t=\tau}}{\sqrt{t-\tau}}\, d\tau, \tag{7.a}$$

$$\Theta(t, 0) = \frac{1}{\sqrt{\pi}\sqrt{\rho c \kappa}} \int_0^t \frac{\dot{q}_s(\tau)}{\sqrt{t-\tau}}\, d\tau. \tag{7.b}$$

Two kind of difficulties arise either for numerical or algebraic approximation of equations (7.a)-(7.b):

(1) The surface temperature $\Theta(t, 0)$ is normally known only at discrete time $t_i$

according with the acquisition frequency of the DAS system.

(2) The computation of $\dot{q}_s(t)$ for a given $\Theta(t,0)$ is not straightforward.

### *5.1 Heaviside like heat flux approximation*

In many practical situation the heat signal $\dot{q}_s(t)$ shows a sudden increase in a short initial time (rise time) and thereafter drops with a approximatively a constant slope. In this situation it is possible to produce, for a given temperature signal, an approximate formula for $\dot{q}_s(t)$. Formula (7.b) can be rewritten as

$$\dot{q}_s(t) + E(t) = \frac{\sqrt{\pi}\sqrt{\rho c \kappa}}{2} \frac{\Theta(t,0)}{\sqrt{t}}, \tag{8}$$

and

$$E(t) = \frac{1}{2\sqrt{t}} \int_0^t \frac{\dot{q}_s(\tau) - \dot{q}_s(t)}{\sqrt{t-\tau}}\, d\tau.$$

where $E(t)$ becomes the absolute error in this approximation if $E(t)$ is neglected. The applications of the above solution requires an accurate determination of the time origin of the parabolic temperature time trace. Moreover, the absolute error $E(t)$ satisfies

$$|E(t)| \leq M_1 \sqrt{\frac{\epsilon}{t}} + M_2, \tag{9}$$

where

$$M_1 = 2 \sup_{x \in [0,\epsilon]} |\dot{q}_s(x)|, \quad M_2 = \sup_{x,y \in [\epsilon,t]} |\dot{q}_s(x) - \dot{q}_s(y)|.$$

The constant $M_1$ is of the order of the maximum recorded heat flux, while the constant $M_2$ is proportional to the heat fluctuation after the initial raise time. It can be noticed in formula (9) that for $t$ small the error is dominated by $M_1\sqrt{\epsilon/t}$ so that approximation (8) is apparently good for $t \gg \epsilon$ and if the rise time $\epsilon$ is short compared to the total test duration. Formula (9) gives a guide rule design for time assessment.

### *5.2 The Cook and Felderman method*

The Cook and Felderman [8] method is based on a piecewise linear approximation of the surface temperature $\Theta(t,0)$ introduced to reconstruct temperature signals known at discrete times. Moreover such an approximation of temperature signal simplifies the approximate computation of integral (7.a). A linear spline $\Theta^L(t)$ which interpolates $\Theta^i = \Theta(t_i,0)$ is build as below:

$$\Theta^L(\tau) = \frac{(\tau - t_{i-1})\Theta^i + (t_i - \tau)\Theta^{i-1}}{t_i - t_{i-1}}, \quad t_{i-1} \le \tau \le t_i. \tag{10}$$

for $i = 1, 2, \ldots, n_s - 1$ where $n_s$ is the total number of sampled temperatures with $t_0 = 0$. Substitution of (10) in formula (7.a) with $t = t_m$ produces an approximate values for $\dot{q}_s(t_m)$. This approximation is known as the Cook and Felderman method. Substituting (10) in (7.a) after few manipulation

$$\dot{q}_s(t_m) = \frac{\sqrt{\rho c \kappa}}{\sqrt{\pi}} \sum_{i=1}^{m} \frac{2(\Theta^i - \Theta^{i-1})}{\sqrt{t_m - t_i} + \sqrt{t_m - t_{i-1}}} + E(t_m), \tag{11}$$

where

$$\begin{aligned} |E(t_m)| \le \frac{\sqrt{\rho c \kappa}}{\sqrt{\pi}} \max_{t\in[0,t_m]} \left| \frac{\partial^2 \Theta(t,0)}{\partial t^2} \right| \\ \times \sum_{i=1}^{m} \frac{(t_i - t_{i-1})^2}{\sqrt{t_m - t_{i-1}} + \sqrt{t_m - t_i}}. \end{aligned} \tag{12}$$

The Cook and Felderman approximation is obtained from (11) by neglecting the error term $E(t_m)$. This last form is the equation usually implemented in heat transfer data reduction programs subjected only to the assumption of the one dimensional heat conduction in a semi-infinite slab with constant thermal properties.

In order to obtain a more simple estimate of $E(t_m)$ by defining $\Delta t = \max_{i=1,2,..,n} t_i - t_{i-1}$ from (12) the following estimate holds

$$|E(t_m)| \le \frac{\sqrt{\rho c \kappa}}{\sqrt{\pi}} \max_{t\in[0,t_m]} \left| \frac{\partial^2 \Theta(t,0)}{\partial t^2} \right| \Delta t \sqrt{t_m},$$

From this inequality it is evident that Cook and Felderman is at least a first order scheme.

**Remark 1** *From* (11) *by setting* $\Theta^{-1} = \Theta^0$ *and* $t_{-1}$ *any number less than* $t_0$ *the*

*following identity follows:*

$$\sum_{i=1}^{m} \frac{\Theta^i - \Theta^{i-1}}{\sqrt{t_m - t_{i-1}} + \sqrt{t_m - t_i}} = \sum_{i=0}^{m-1} \left( \frac{\Theta^{i+1} - \Theta^i}{t_{i+1} - t_i} - \frac{\Theta^i - \Theta^{i-1}}{t_i - t_{i-1}} \right) \sqrt{t_m - t_i} \tag{13}$$

*when sampling rate is constant i.e.* $t_i - t_{i-1} = \Delta t$ *for all* $i$ *equation* (13) *substituted in* (11) *reduce to*

$$\boxed{\dot{q}_s(t_m) \approx \frac{2\sqrt{\rho c \kappa}}{\sqrt{\pi}\sqrt{\Delta t}} \sum_{i=0}^{m-1} \left( \Theta^{i+1} - 2\Theta^i + \Theta^{i-1} \right) \sqrt{m-i}}$$

*which is the scheme differently deduced by Oldfield* et al. *[21].*

### *5.3 Implicit Cook and Felderman*

An implicit version of Cook and Felderman is based on a piecewise constant approximation of the surface heat $\dot{q}_s(t)$. A piecewise constant spline $\dot{q}^L(t)$ is build as below:

$$\dot{q}^L(\tau) = \dot{q}_{s_{i-\frac{1}{2}}}, \quad t_{i-1} \le \tau \le t_i. \tag{14}$$

Substitution of (14) in formula (7.b) instead of $\dot{q}_s(t)$ produce for $t = t_m$ an approximate values for $\Theta(t_m, 0)$.

$$\Theta(t_m, 0) \approx \Theta^m = 2 \sum_{i=1}^{m} \frac{\sqrt{t_m - t_{i-1}} - \sqrt{t_m - t_i}}{\sqrt{\pi}\sqrt{\rho c \kappa}} \dot{q}_{s_{i-\frac{1}{2}}},$$

which for all $m > 0$ is an implicit linear relation in the unknown $\dot{q}_{s_{i-\frac{1}{2}}}$ that can be resolved assuming $\Theta(t_m, 0) = \Theta^m$ by a simple recurrence.

## 6 Two layer slab

If the test duration is short enough and/or the thickness of the slab is properly chosen the finite size second layer, can be approximated by a semi-infinite one. According to the consideration in section 5, if the temperature inside the slab does not increase too much the following assumption can be done

$$\rho_i(\Theta) \equiv \rho_i, \quad c_i(\Theta) \equiv c_i, \quad \kappa_i(\Theta) \equiv \kappa_i, \quad i = 1, 2 \tag{15}$$

i.e. their values are assumed constant and evaluated at the initial temperature.
The one dimensional semi-infinite slab can be modeled by equations (2) with $\ell = \infty$ and $m = 2$. The slab is assumed to be in thermal equilibrium at time $t = 0$, so that (without loss of generality) we assume $\Theta(0, z) = 0$ for all $z \geq 0$. With assumption (15) the equations (2) are linear and can be solved by means of the Laplace transform and $\overline{\dot{q}_s}(s)$ can be correlated with $\overline{\Theta}(s, 0)$ as follows

$$\frac{\sqrt{\pi}\,\dot{q}_s(t)}{\sqrt{\rho_1 c_1 \kappa_1}} = \int_0^t \left.\frac{\partial \Theta(t,0)}{\partial t}\right|_{t=\tau} \frac{\Omega\left(-A, t-\tau\right)}{\sqrt{t-\tau}}\, d\tau, \tag{16.a}$$

$$\Theta(t,0) = \frac{1}{\sqrt{\pi}\sqrt{\rho_1 c_1 \kappa_1}} \int_0^t \dot{q}_s(\tau) \frac{\Omega\left(A, t-\tau\right)}{\sqrt{t-\tau}}\, d\tau, \tag{16.b}$$

where

$$\Omega\left(\sigma, x\right) = 1 + 2\sum_{n=1}^{\infty} \sigma^n \exp\left(-\frac{n^2 \tau_1}{x}\right),$$

$$A = \frac{\sqrt{\rho_1 c_1 \kappa_1} - \sqrt{\rho_2 c_2 \kappa_2}}{\sqrt{\rho_1 c_1 \kappa_1} + \sqrt{\rho_2 c_2 \kappa_2}}, \quad \tau_1 = \frac{z_1^2}{\alpha_1}.$$

Notice that in the case $\sigma = 0$ the function $\Omega\left(\sigma, x\right)$ is identically equal to $1$. Observe that when $A = 0$ the two layer slab behaves as a single layer. This is the case when the two layers are made of the same materials or when they have the same thermal product.

### *6.1 Heaviside like heat flux approximation for two layer slab*

When a sudden change of the thermo-fluid dynamic characteristics of the free stream occurs it is possible to produce, for a given temperature signal, an approximate formula for $\dot{q}_s(t)$. Formula (16.b) can be rewritten as

$$\begin{aligned}\sqrt{\pi}\sqrt{\rho_1 c_1 \kappa_1}\Theta(t,0) = 2\sqrt{t}E(t) + \dot{q}_s(t)\Big\{2\sqrt{t} + \\ 4\sum_{n=1}^{\infty} A^n \left[\sqrt{t}\exp\left(-(nz)^2\right) + n\sqrt{\tau_1}\sqrt{\pi}\,\mathrm{erf}\left(nz\right)\right]\Big\},\end{aligned} \tag{17}$$

where $z = \tau_1/t$ and

$$E(t) = \frac{1}{2\sqrt{t}} \int_0^t \frac{\dot{q}_s(\tau) - \dot{q}_s(t)}{\sqrt{t-\tau}} \Omega\left(A, t-\tau\right) d\tau.$$

Following Pelle and Arts [22], relation (17) can be roughly approximated by:

$$\dot{q}_s(t) \approx \Theta(t,0) \times \begin{cases} \left[\frac{2\sqrt{t}}{\sqrt{\pi}\sqrt{\rho_1 c_1 \kappa_1}}\right]^{-1} & t < t^* \\ \left[\frac{2\sqrt{t}}{\sqrt{\pi}\sqrt{\rho_2 c_2 \kappa_2}} + \frac{z_1}{\kappa_1}\left(1 - \frac{\rho_1 c_1 \kappa_1}{\rho_2 c_2 \kappa_2}\right)\right]^{-1} & t > t^* \end{cases},$$

where

$$t^* = \frac{\sqrt{\pi}}{2}\frac{z_1}{\kappa_1}\frac{\sqrt{\rho_1 c_1 \kappa_1}}{\sqrt{\rho_2 c_2 \kappa_2}}.$$

### *6.2 A Cook and Felderman like method*

As for the Cook and Felderman method the surface temperature $\Theta(t,0)$ is approximated by a linear spline as in (10). Substitution of (10) in formula (16.a) produces

$$\dot{q}_s(t_m) = \frac{\sqrt{\rho_1 c_1 \kappa_1}}{\sqrt{\pi}} \sum_{i=1}^{m} C_{i-\frac{1}{2}}^m \left(\Theta^i - \Theta^{i-1}\right) + E(t_m) \tag{18}$$

where $C_{i-\frac{1}{2}}^m = (D_{i-1}^m - D_i^m)/(t_i - t_{i-1})$ and

$$D_i^m = 2\sqrt{t_m - t_i} + 4\sum_{n=1}^{\infty}(-A)^n \left(\sqrt{t_m - t_i}\exp\left(-\frac{n^2\tau_1}{t_m - t_i}\right) + n\sqrt{\tau_1}\sqrt{\pi}\,\mathrm{erf}\left(n\frac{\sqrt{\tau_1}}{\sqrt{t_m - t_i}}\right)\right)$$

The Cook and Felderman like approximation is obtained from (18) by neglecting the error term $E(t_m)$. The error $E(t_m)$ becomes the absolute error of Cook and Felderman like approximation. An upper bound of this error can be estimated as follows

$$|E(t_m)| \le \Delta t \frac{\sqrt{\rho_1 c_1 \kappa_1}}{\sqrt{\pi}} \max_{t\in[0,t_m]}\left|\frac{\partial^2\Theta(t,0)}{\partial t^2}\right| \times \left[C\sqrt{t_m} + \frac{\sqrt{\pi}\sqrt{\tau_1}}{2}(C^2 - 1)\right],$$

where

$$C = \frac{\max\left\{\sqrt{\rho_1 c_1 \kappa_1}, \sqrt{\rho_2 c_2 \kappa_2}\right\}}{\min\left\{\sqrt{\rho_1 c_1 \kappa_1}, \sqrt{\rho_2 c_2 \kappa_2}\right\}}, \quad \Delta t = \max_{i=1,2,..,n} t_i - t_{i-1}$$

so it is clear that it is at least a first order scheme.

**Remark 2** *The computation of $C_{i-\frac{1}{2}}^m$ is very expensive due to the presence of a*

*series and the error function erf*$(\cdot)$*. By Lagrange and mean theorem* $C^m_{i-\frac{1}{2}}$ *can be approximated by:*

$$(z_i + z_{i-1})\, C^m_{i-\frac{1}{2}} \approx 2 + 4 \sum_{n=1}^{\infty} (-A)^n exp\left( -\frac{n^2 \tau_1}{z_i z_{i-1}} \right), \tag{19}$$

*where* $z_i = \sqrt{t_m - t_i}$ *and for* $i = 1$ *equation* (19) *becomes* $C^m_{\frac{1}{2}} \approx 2/z_1$.

### *6.3 Implicit Cook and Felderman like method*

A piecewise constant spline $\dot{q}^L(t)$ is build as in (14) and by substitution of (14) in formula (16.b) instead of $\dot{q}_s(t)$ produce for $t = t_m$ an approximate values for $\Theta(t_m, 0)$. The result is the following:

$$\begin{aligned} \Theta(t_m, 0) \approx \Theta^m &= \frac{\sqrt{\rho_1 c_1 \kappa_1}}{\sqrt{\pi}} \sum_{i=1}^{m} (t_i - t_{i-1}) I^m_{i-\frac{1}{2}} \dot{q}_{s\,i-\frac{1}{2}}, \\ (z_i + z_{i-1}) I^m_{i-\frac{1}{2}} &= 2 + 4 \sum_{n=1}^{\infty} A^n \exp\left( -\frac{n^2 \tau_1}{z_i z_{i-1}} \right), \end{aligned} \tag{20}$$

which for all $m > 0$ is an implicit linear relation in the unknown $\dot{q}_{s\,i-\frac{1}{2}}$. Assuming $\Theta(t_m, 0) \approx \Theta^m$ in (20) we obtain an implicit formulation for $\dot{q}_{s\,i-\frac{1}{2}}$ which can be solved by a simple recurrence.

### *6.4 The Finite Element numerical scheme*

The Finite Element method is widely used for the solutions of many kind of PDE [27] such as the parabolic ones in (2). This method is based on the approximation of the solution in a finite dimensional subspace, typically piecewise polynomials. In the present case the finite dimensional subspace is constructed as the space of piecewise linear splines in a partition of the interval $[0, \ell]$. The interval $[0, \ell]$ is partitioned in $n$ subintervals not necessarily of the same size,

$$0 = z_0 < z_1 < z_2 < \cdots < z_{n-1} < z_n = \ell. \tag{21}$$

The partition (21) is chosen in such a way that inside the intervals $[z_{i-1}, z_i]$ the functions $\kappa(z, \Theta)$, $\rho(z, \Theta)$ and $c(z, \Theta)$ are constant with respect to $z$ so that the slab can be considered as made of $n$ layers. In general $n > m$ so that many of the original layers are split in others layers. Denoting with $\rho_i$, $c_i$ and $\kappa_i$ the corresponding

function on the layer then

$$\rho(z,\Theta)=\rho_i(\Theta),\quad c(z,\Theta)=c_i(\Theta),\quad \kappa(z,\Theta)=\kappa_i(\Theta),$$

for $i=1,2,\ldots,n$ and $z_{i-1}<z<z_i$. The temperature $\Theta(t,z)$ is approximated by using expansion

$$\Theta(t,z)\approx\sum_{i=0}^{n}\Theta_i(t)\phi_i(z),$$

where $\phi_i$ are standard piecewise linear functions. By using finite elements approximation for (2) with boundary condition (5) and (4) the following ODE is obtained:

$$\begin{aligned}&\Theta_0(t)=\Theta^s(t),\\&\sum_{i=0}^{n}\Theta_i'(t)A_{ij}(\Theta)+\sum_{i=0}^{n}\Theta_i(t)B_{ij}(\Theta)=0,\quad j=1,2,\ldots,n.\end{aligned}\tag{22}$$

The coefficients $A_{ij}$ and $B_{ij}$ results as following:

$$\begin{aligned}A_{ij}(\Theta)&=\int_0^{\ell}\rho\left(z,\Theta(t,z)\right)c\left(z,\Theta(t,z)\right)\phi_i(z)\phi_j(z)\,dz,\\B_{ij}(\Theta)&=\int_0^{\ell}\kappa\left(z,\Theta(t,z)\right)\phi_i'(z)\phi_j'(z)\,dz.\end{aligned}\tag{23}$$

A trapezoidal quadrature rule is used instead of exact integrals for (23). The same $A_{ij}$ and $B_{ij}$ are used to denote such an approximation and take the values:

$$A_{ij}(\Theta)=\begin{cases}M_i(\Theta_i) & \text{if } i=j\\ 0 & \text{otherwise}\end{cases},$$

$$B_{ij}(\Theta)=\begin{cases}-M_{i\pm\frac{1}{2}}(\Theta_i,\Theta_{i\pm1}) & \text{if } j=i\pm1\\ M_{i+\frac{1}{2}}(\Theta_i,\Theta_{i+1}))+M_{i-\frac{1}{2}}(\Theta_{i-1},\Theta_i) & \text{if } j=i\\ 0 & \text{otherwise}\end{cases},$$

where

$$\begin{aligned}M_0(\Theta_0)&=\rho_0(\Theta_0)c_0(\Theta_0)(z_1-z_0)/2,\\M_i(\Theta_i)&=(\rho_{i-1}(\Theta_i)c_{i-1}(\Theta_i)(z_i-z_{i-1})\\&\qquad+\rho_i(\Theta_i)c_i(\Theta_i)(z_{i+1}-z_i))/2,\\M_n(\Theta_n)&=\rho_{n-1}(\Theta_n)c_{n-1}(\Theta_n)(z_n-z_{n-1})/2,\\M_{i+\frac{1}{2}}(\Theta_i,\Theta_{i+1})&=\left(\kappa_i(\Theta_i)+\kappa_i(\Theta_{i+1})\right)/(2(z_{i+1}-z_i)),\end{aligned}$$

Equations (22) is a semi-discrete approximation of equation (2) and constitute a large system of initial value ordinary differential equations (ODE).

### *6.5 Time semi-implicit integrator*

To solve system (22) any standard scheme for initial value ODE can be used. A simple scheme is the forward Euler scheme but applied to ODE (22) can produce temperature oscillations. A simple modification of the implicit Euler scheme results in a relatively cheap stable scheme. The resulting scheme, by using the following shortcut

- $\Theta_i^k$ the approximation of $\Theta_i(t_k)$;
- $A_{ij}^k = A_{ij}(\Theta^k)$;
- $B_{ij}^k = B_{ij}(\Theta^k)$;
- $\Delta t_j = t_{j+1} - t_j$

is the following

$$\Theta_0^{k+1} = \Theta^s(t^{k+1}),$$
$$\sum_{i=0}^{n} A_{ij}^k \frac{\Theta_i^{k+1} - \Theta_i^{k+1}}{\Delta t_j} + \sum_{i=0}^{n} B_{ij}^k \Theta_i^{k+1} = 0$$

for $j = 1, 2, \ldots, n$. It is easy to see that the solution step involves the solution of a strictly diagonally dominant tridiagonal system with positive elements on the diagonal and non negative elements elsewhere. Then the coefficient matrix of the system is an M-matrix (see e.g. Axelsson [2] for the definition). It is easy to prove that the discrete solution satisfies the discrete maximum principle [5] so that the scheme is unconditionally stable.

### *6.6 Choice of the mesh and experiment design*

Consider the heat equation for a single layer where the physical parameters are independent from the temperature:

$$\frac{\partial}{\partial t}\Theta(t,z) = \frac{\kappa}{\rho c}\frac{\partial^2}{\partial z^2}\Theta(t,z)$$

the numerical scheme previously introduced is $1^{st}$ order in time and $2^{nd}$ order in space i.e. it has an error of the form:

$$E_S \Delta t + E_M \Delta z^2 \tag{24}$$

where $\Delta t = 1/f_s$, $f_s$ being the sampling frequency and $\Delta z$ is the maximum size of the Finite Elements cells. From (24) the total error depends on two different contributions:

- An error due to the sampling frequency $f_s$; here referred as sampling error $S_E = E_S \Delta t$;
- An error due to the spatial discretization $\Delta z$; here referred as mesh error $M_E = E_M \Delta z^2$;

Consider the parameter

$$\mathcal{A} = \frac{E_S}{E_M} \frac{\Delta t}{\Delta z^2}$$

when $\mathcal{A} \gg 1$ it means that the error is dominated by the low sampling rate or by an excessive fine mesh. When $\mathcal{A} \ll 1$ it means that the error is dominated by the coarse mesh or by an excessive sampling rate. The parameter $\mathcal{A}$ can be used to optimize the mesh definition with respect to the sampling frequency.

Normally the sampling rate is somehow determined by the hardware, so that from (24) the sampling error $S_E$ bounds the maximum achievable accuracy.

The mesh definition is normally chosen in order to introduce a mesh error $M_E$ of the same order of the sampling error $S_E$. However the sampling error is, in many practical applications, lower than the error introduced by parameter uncertainty (i.e. the values of the physical properties of the substrate given from the manufacturer, temperature measurement and so on). From the point of view of the experiment designer it is evident that mesh can be coarsened according to such an inaccuracy level.

It is worth to analyze the behavior of the error (24) as the sampling rate goes to $\infty$ and the parameter $\mathcal{A}$ is fixed. From this hypothesis and (24) the error becomes

$$\frac{E_S}{f_s}\left(1 + \frac{1}{\mathcal{A}}\right) \quad \text{and} \quad \Delta z = \sqrt{\frac{E_S}{E_M}\frac{1}{f_s}},$$

The cost of each advancing step is proportional the mesh size which is in turn proportional to $1/\Delta z$; the total number of steps being proportional to $1/f_s$ the total cost is proportional to $f_s^{3/2}$ while the accuracy from (24) is proportional to $1/f_s$.

Because the total number of samples $n_s \propto f_s$ the computational cost is $\mathcal{O}\left\{n_s^{3/2}\right\}$ and accuracy is $\mathcal{O}\left\{1/n_s^2\right\}$ so that although the computational cost is apparently asymptotically high the cost versus accuracy is not so bad.

However we observe that the computational effort is extremely low also in real test cases where $n_s \propto 10^4$ and for them the running time on a small PC is a few tens of seconds.

Moreover the finite elements approach permits to treat easily also the nonlinear cases when the temperature dependence of the physical properties cannot be neglected. Such an extension is not straightforward for methods based on transformations.

## 7 Numerical Results

### *7.1 Code validation*

In order to validate the presented approach an ideal signal has been used having a know solution in the case of a semi-infinite slab with constant physical properties. This signal has been derived from the following expression of the impinging heat flux [15]

$$\dot{q}_s(t) = \begin{cases} 0 & t < 0 \\ A + B\cos 2\pi f_q t + \phi & t \geq 0 \end{cases} \tag{25}$$

where $A$ is the step magnitude, $B$ is the superimposed signal magnitude, $f_q$ is the frequency of the superimposed signal and $\phi$ is the phase of the superimposed signal.

The surface temperature history which generates such an heat flux is

$$\begin{aligned}\sqrt{\pi}\,\sqrt{\rho c\kappa}\;\;\Theta^s(t) = 2A\sqrt{t}\\ +\frac{B}{\sqrt{f_q}}\cos 2\pi f_q t + \phi \mathrm{F}_c\left(2\sqrt{f_q t}\right)\\ +\frac{B}{\sqrt{f_q}}\sin 2\pi f_q t + \phi \mathrm{F}_s\left(2\sqrt{f_q t}\right)\end{aligned} \tag{26}$$

and is valid with the above mentioned assumptions. The heat flux has been reconstructed from temperature signal (26) using the two formulations of the Cook and Felderman method (implicit and standard one) and the finite element code with various signal frequencies $f_q$ and different sampling rates $f_s$. Both single and double layer configurations have been tested according to the approaches of sections 5 and 6. The test cases are listed in Table 1.

Cases form $1$ to $6$ are related to the single layer thin film having macor® as substrate. The thickness of the layer was $5\,mm$ and the test duration was $1s$. Figure 4 shows the solution of test cases $1$, $2$ and $3$ when temperature signal given in (26) is applied. A step like temperature signal is produced in the flow stream. Results are presented in terms of non dimensional heat flux (ratio of actual heat flux $Q$ by the expected heat flux $A$) and non dimensional time scale ($t \cdot f_s$) for the three test cases. After a short initial time all methods give an excellent reconstruction. The implicit Cook and Felderman response seems to reconstruct the heat Heaviside signal better than Finite Elements and standard Cook and Felderman. The initial peak is suppressed. Notice that in the initial part of the signal (step region) the Finite Element code reconstructs better than the standard Cook and Felderman but worse than the implicit Cook and Felderman. The higher the sampling frequency, the faster the heat flux traces approach the actual value.

For a given accuracy requirement the size of the Finite Element mesh results fixed according to the considerations of section 6.6. The computational effort grows therefore linearly with frequency, while the better implementation of Cook and Felderman has an higher grow rate. Thus the Finite Element results are cheaper than Cook and Felderman when data reduction of a large data set is performed.

In Figure 5 (test cases $4$, $5$ and $6$ of Table 1), solution of (26) is given respectively for $f_s/f_q = 2.5, 25, 50$ and $B/A = 0.5$. The highest over estimation of the heat flux

| **single layer** | | | | |
|---|---|---|---|---|
| test | $A[W/m^2]$ | $B[W/m^2]$ | $f_q[Hz]$ | $f_s[Hz]$ |
| 1 | 1000 | 0 | 0 | 10 |
| 2 | 1000 | 0 | 0 | 100 |
| 3 | 1000 | 0 | 0 | 1000 |
| 4 | 1000 | 500 | 4 | 10 |
| 5 | 1000 | 500 | 4 | 100 |
| 6 | 1000 | 500 | 4 | 1000 |
| **double layer** | | | | |
| test | $A[W/m^2]$ | $B[W/m^2]$ | $f_q[Hz]$ | $f_s[Hz]$ |
| 7 | 1000 | 0 | 0 | 10 |
| 8 | 1000 | 0 | 0 | 100 |
| 9 | 1000 | 0 | 0 | 1000 |
| 10 | 1000 | 500 | 4 | 10 |
| 11 | 1000 | 500 | 4 | 100 |
| 12 | 1000 | 500 | 4 | 1000 |

Table 1

is due, analogously to the first $3$ presented cases to standard Cook and Felderman. The signal reconstruction is poor for $f_s/f_q = 2.5$ for all methods. The step is perfectly obtained from the implicit method. The Higher ratio $f_s/f_0$, the better is the reconstruction of the oscillating part of the signal, however already at $f_s/f_q = 25$ the reconstruction is very good in maximum amplitude and phase.

In order to validate the code in the case of the double layer feature, the Finite Element discretization has been used to compute $\Theta^s(t)$ from (25). $\dot{q}_s(t)$ has been afterwards reevaluated with the finite element and Cook and Felderman methods.

Step like heat functions results (test cases $7$, $8$ and $9$ of table 1) are given in Figure 6.

Values of

$$\frac{\sqrt{\rho_1 c_1 \kappa_1}}{\sqrt{\rho_2 c_2 \kappa_2}} \approx 0.04$$

and (see Figure 2) $a/(b-a) \approx 10^4$ for the layers thickness ratio have been adopted. The maximum test duration was $1\,s$. The standard Cook and Felderman overestimates the actual heat flux. The absence of peak in the Finite Element solution is essentially due to the procedure used to obtain the testing signals. On the same frequency base, longer times are necessary to approach the expected value of the heat flux compared to single layer cases. Oscillating test cases are depicted in Figures 7. Excellent reconstruction is performed for $f_s/f_q$ ratio bigger than $25$. Computational cost saves result to be even more evident than single layer case when the Finite Element code is adopted.

### *7.2 Experimental heat flux data reduction*

The Finite Element solution technique was finally used to process raw data obtained from experimental test facilities. In order to assess the performance for signals having different characteristics, four surface temperature histories have been selected. The test cases are listed in Table 2. Figure 8a shows a typical temperature signal ob-

| test | Facility – Location |
|---|---|
| 13 | Low Speed Tunnel – Trento University, Italy |
| 14 | CT2 Light Piston Isentropic Compression Tube – VKI, Belgium |
| 15 | H3 Mach 6 wind tunnel – VKI, Belgium |
| 16 | H3 wind tunnel – VKI, Belgium |

Table 2

tained in the short duration low speed tunnel (Mach $< 0.1$) of the turbomachinery lab of the University of Trento. An upilex® layer of $75\,\mu m$ was used, bounded on a plexiglass® wall of $15\,mm$ thickness as supporting substrate. The film was placed on the midpoint of the floor between two consecutive ribs. Further details are given in Battisti and Schmeer [4]. The sampling frequency was $500$Hz. Because of the

very noisy temperature signal, high scatter appears in heat flux reduction trace in the Finite Element and both Cook and Felderman methods (Figure 8c–d). Due to the summation in equation (11) and (20) these methods takes the longest CPU time for large $n_s$.

The second investigated signal is taken from measurements performed in the Light Piston Isentropic Compression Tube facility (CT2) at the von Karman Institute. Details of the experimental rig and the sensor are given in Pelle and Arts [22]. The temperature signal belongs to a single layer thin film (platinum over macor®) placed well down stream of the tripping wire of a flat plate. The sensor was subjected to a Mach $0.6$ short duration flow stream. The surface temperature history is depicted in Figure 9a. The three processing methods are reported in Figure 9b-d. A good agreement results from their comparison.

The third test case was a compression ramp in the H3 Mach 6 wind tunnel of the von Karman Institute. Single layer thin film (platinum over macor®) was used. Figure 10a shows the temperature evolution of the upper and lower faces of a machined macor® model. Data were sampled at $250$Hz. The model was injected in the Mach 6 flow having a free stream temperature of about $520K$. Further details are given in Marquet and Charbonnier [18]. The Figure 10b shows the result obtained with the Finite Element code. A similar solution method was used at the von Karman Institute for data reduction and the two solutions (here not reported for seek of brevity) do not show any consistent difference. The lower pictures 10c-d show respectively the same temperature signal and the corresponding heat flux solution but performed when a sampling rate of $25$Hz instead of the original $250$Hz are used. Apart from the inherent noise filtration effect, the Finite Element code seems to yield (as expected from the previous validation results) an accurate heat flux reconstruction.

When the model back surface temperature significantly changes during the test, the semi-infinite assumption is no longer valid and the Cook and Felderman like techniques cannot be safely used. Moreover, if the model body even experiences significant temperature rise, constant physical properties assumption can introduce further errors in the solution. If this is the case both analog and Cook and Felderman methods are not accurate and numerical discretization are forced. In Figure 11a a typical example is presented. Temperature histories of the upper and lower sur-

face of the same model of test case $15$ measured by means of single layer thin films (platinum over macor®). The model was first heated up to $550K$ by infrared lamps, successively the lamps were switched off and the model was injected in vacuum. Figure 11b shows the corresponding heat flux signal obtained by using the Finite Elements code implemented with constant physical properties. Absolute differences are less then $10^{-3}$ respect to the solution obtained at the von Karman Institute. When temperature variable properties are considered, a small difference between the two solution becomes evident and results in a slightly overestimation of the heat flux during the heating phase and under estimation during the cooling one (as shown in Figure 11c). The maximum is of about $2.5\%$ when an heat flux of about $200000\,W/m^2$ impinges.

## 8 Conclusions

Common data reduction procedure for heat transfer measurements in short duration facilities by means of single and double layer thin film, have been reviewed and discussed. A simple Finite Element discretization has been implemented and its ability to accurately reconstruct signals of known testing functions (as Heaviside signal with superimposed fluctuations) has been checked. Experimental, not filtered, data with various sampling frequencies and flow characteristics have been processed. The implementation of temperature variable physical properties of the body has been discussed for a typical test case when its influence on accuracy cannot be neglected. Results seem to confirm the very good performance of the code which shows a very accurate signal reconstruction also at very low sampling frequencies. When the semi-infinite slab assumption is no longer valid (i.e. leading edge of blades) numerical discretization such as Finite Element approach is not negotiable. Further improvement of the code will be the development of a 2-D scheme in order to consider problems where lateral conduction effects cannot be neglected, and the evaluation of the influence of heat flux generated by Joule effect into the sensor.

## 9 Acknowledgments

We thankful acknowledge professor T. Arts and professor J. M. Charbonnier of the von Karman Institute for useful discussions and for providing us the experimental data.

## References


[1] R. W. Ainsworth, J. L. Allen, M. R. D. Davies, and J. E. D. et al., *Developments in instrumentation and processing for transient heat transfer measurement in a full stage model turbine*, Transaction of ASME, **111** (1989) 20–27.

[2] O. Axelsson, **Iterative Solution Methods** (Cambridge University Press, 1994).

[3] L. Battisti and T. Arts, *Wall heat transfer measurements in rib-roughened cooling channels by means of a transient technique*, ATI $51^0$ Convegno ATI, Udine 16–20 Settembre (1996) 811–822.

[4] L. Battisti and T. Schmeer, *Experimental study of the surface heat transfer enhancement in a rib roughened blade coolant channel by means of double layer thin films*, Proceedings of the $55^o$ Eurotherm Seminar, Santorini, Greece.

[5] E. Bertolazzi, *Numerical conservation and discrete maximum principle for elliptic pdes*, Mathematical Models and Methods in Applied Sciences, **8** (1998) 685–711.

[6] C. Camci and T. Arts, *Experimental heat transfer investigation around the film cooled leading edge of a high pressure gas turbine rotor blade*, ASME Paper n. 85-GT-114 Houston Texas.

[7] H. Consigny and B. E. Richard, *Short duration measurement of heat transfer rate to a gas turbine rotor blade*, Journal of Engineering for Power, **104** (1982) 542–551.

[8] W. J. Cook and E. J. Felderman, *Reduction of data from thin film heat transfer gauges: A concise numerical technique*, AIAA Journal, **4** (1966) 561–562.

[9] T. E. Diller, **Advances in Heat Transfer Vol 23** (Academic Press, 1991).

[10] J. E. Doorly, *Procedures to determining surface heat flux using thin film gauges on a coated metal model in a transient test facility*, ASME, 87-GT-95.

[11] J. E. Doorly and M. L. G. Oldfield, *The theory of advanced multi-layer thin film heat transfer gauges*, Int. J.Heat Mass Transfer, **30** (1987) 1159–1168.

[12] M. G. Dunn, *Phase and time resolved measurement of unsteady heat transfer and pressure in a full-stage rotating turbine*, ASMEe Paper n. 89-GT-135.

[13] M. G. Dunn and A. Hause, *Measurement of the heat flux and pressure in a turbine stage*, ASME Journal of Engineering for Power, **104** (1981) 215–223.

[14] M. G. Dunn, H. L. Martin, and M. J. Stanek, *Heat flux and pressure measurement and comparison with prediction for a low aspect ratio turbine stage*, ASME Journal of Turbomachinery, **108** (1986) 108–115.

[15] W. K. George, W. J. Rae, and S. H. Woodward, *An evaluation of the analog and numerical techniques for unsteady heat transfer measurement with thin film gauges in transient facilities*, Experimental Thermal and Fluid Science, **4** (1991) 332–342.

[16] S. M. Guo, M. C. Spencer, G. D. Lock, and T. V. Jones, *The application of thin film gauges on flexible plastic substrate to the gas turbine situation*, Paper offered for 1995 ASME Turbo Expo, Huston, USA.

[17] J. Lukasiewicz, **Experimental Methods in Hypersonic** (Marcel Dekker, 1973).

[18] B. Marquet and J. M. Charbonnier, *Shock wave boundary layer interaction on hot surfaces: Analisys of the results of the thest campaign for the study of wall temperature effects*, Technical Note GSTP1-TR-6501-VKIN.

[19] B. Marquet and J. M. Charbonnier, *Shock wave boundary layer interaction on hot surfaces: Pressure and heat transfer measurements on hot wall compression ramp models at mach 6*, Technical Note GSTP1-TR-6301-VKIN.

[20] R. F. Meyer, *A heat flux meter for use with thin film surface thermometers*, NRC Canada, Aero Rep. LR279.

[21] M. L. G. Oldfield, T. V. Jones, and D. L. Schultz, *On-line computer for transient turbine cascade instruments*, IEEE Transactions on Aerospace and Electronic Systems AES-14, **5**.

[22] O. Pelle and T. Arts, *Development of a double layer thin film gauge for surface heat transfer measurement*, Proceedings of the $55^0$ Eurotherm Seminar, Santorini, Greece.

[23] A. Pope and K. L. Goin, **High Speed Wind Tunnel Testing** (Wiley and Sons, 1965).

[24] D. L. Schultz and T. V. Jones, *Heat transfer in short duration hypersonic facilities*, AGARD AG 165.

[25] J. P. Vermeulen and G. Simeonides, *Parametric studies of shock wave /boundary layer interactions over 2-d compression corners at mach 6*, VKI Technical Note 181.

[26] R. J. Vidal, *Model instrumentation technique for heat transfer and force mea-*

*surements in a hypersonic shock tunnel*, C.A.L. report AD-917-A-1.

[27] O. C. Zienkiewicz and R. L. Taylor, **The Finite Element Method** (Mc Graw Hill, 1989).

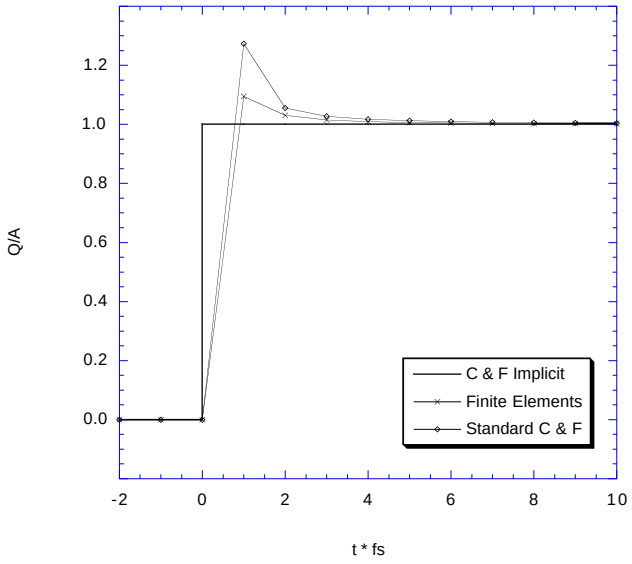


Fig. 4. Single layer heat flux reconstruction (tests 1, 2, 3)

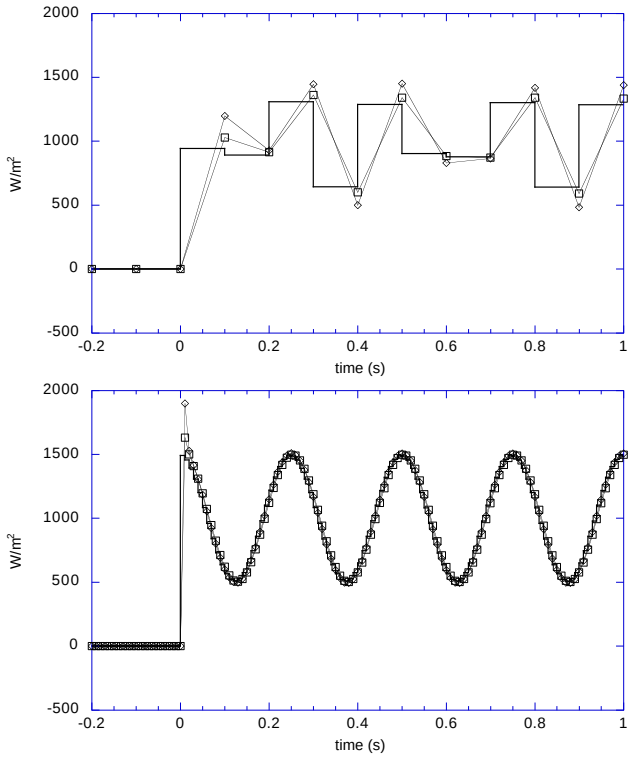


Fig. 5. Oscillating signal reconstruction for single layer configuration (tests 4, 5, 6)

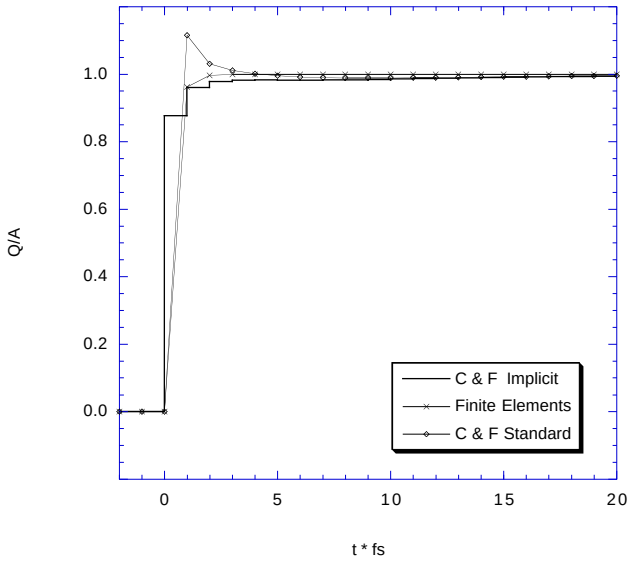


Fig. 6. Double layer heat flux reconstruction (tests 7, 8, 9)

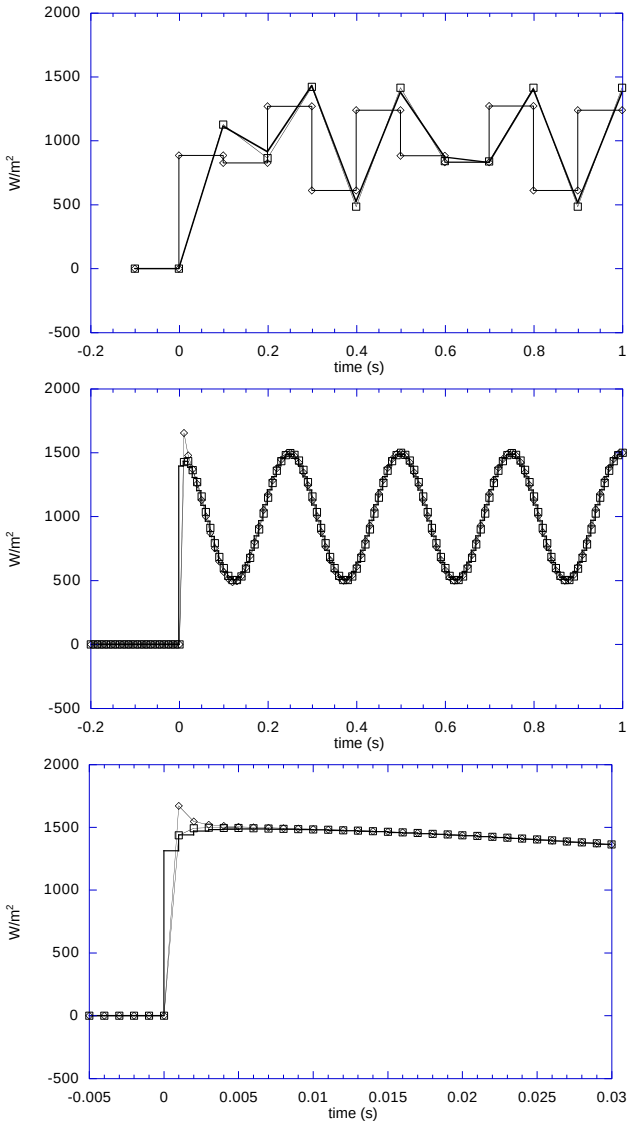


Fig. 7. Oscillating signal reconstruction for double layer configuration (tests 10, 11, 12)

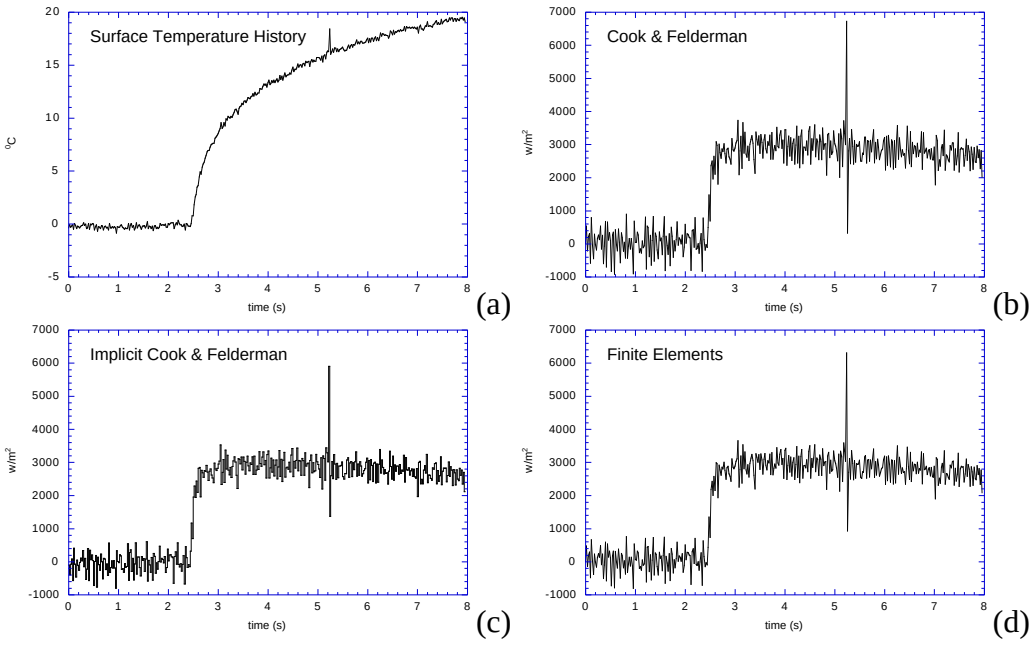


Fig. 8. Double layer thin film surface temperature signal and heat flux computation for test case 13

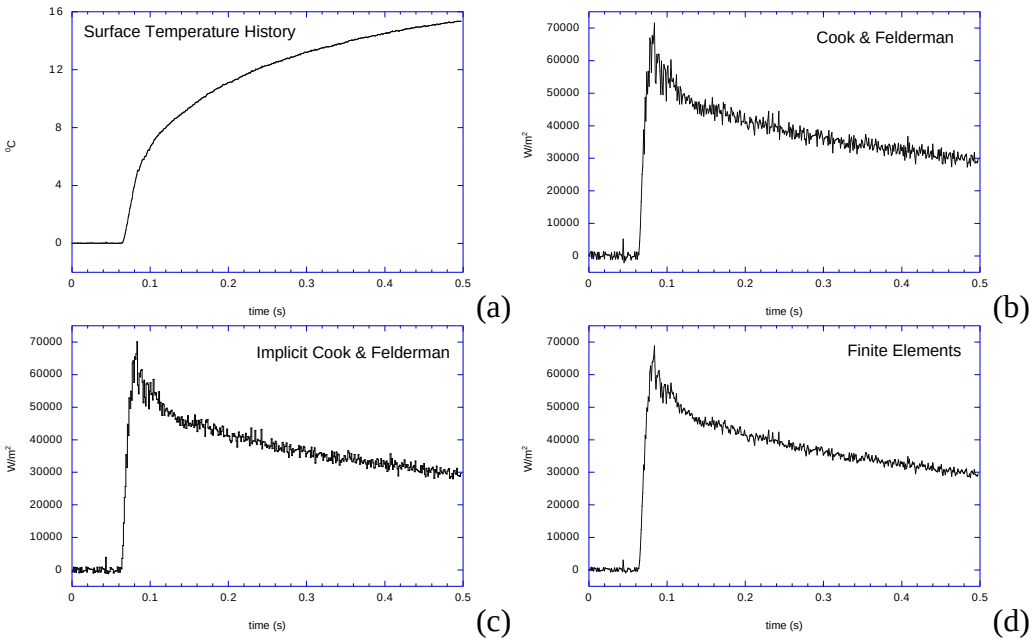


Fig. 9. Single layer thin film surface temperature signal and heat flux computation for test case 14 at Mach 0.9

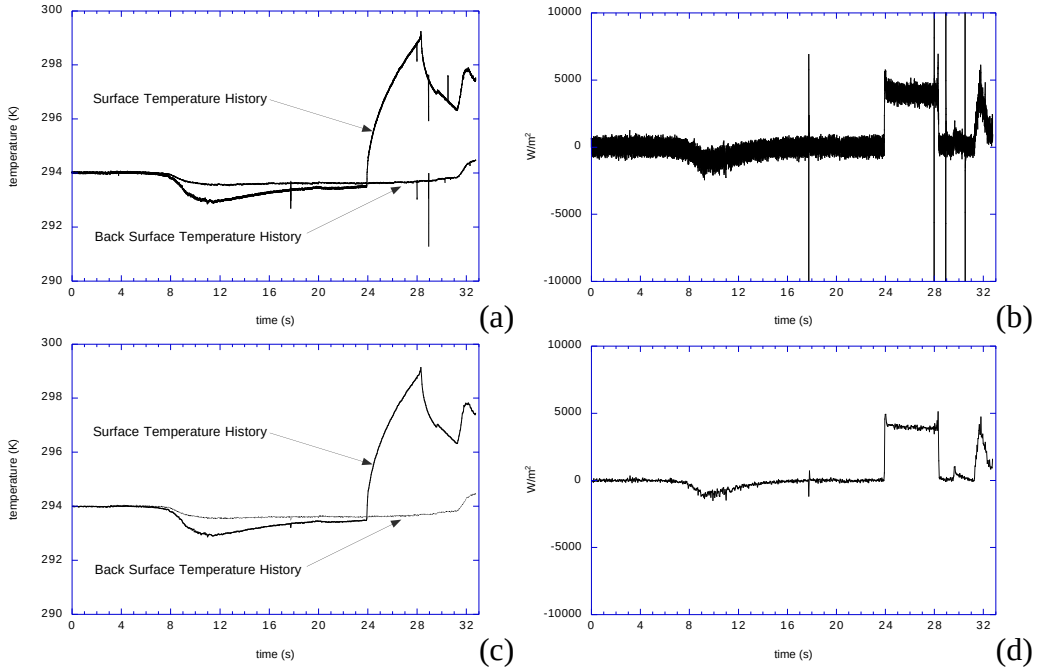


Fig. 10. Single layer thin film surface temperature signal and heat flux computation for test case 15

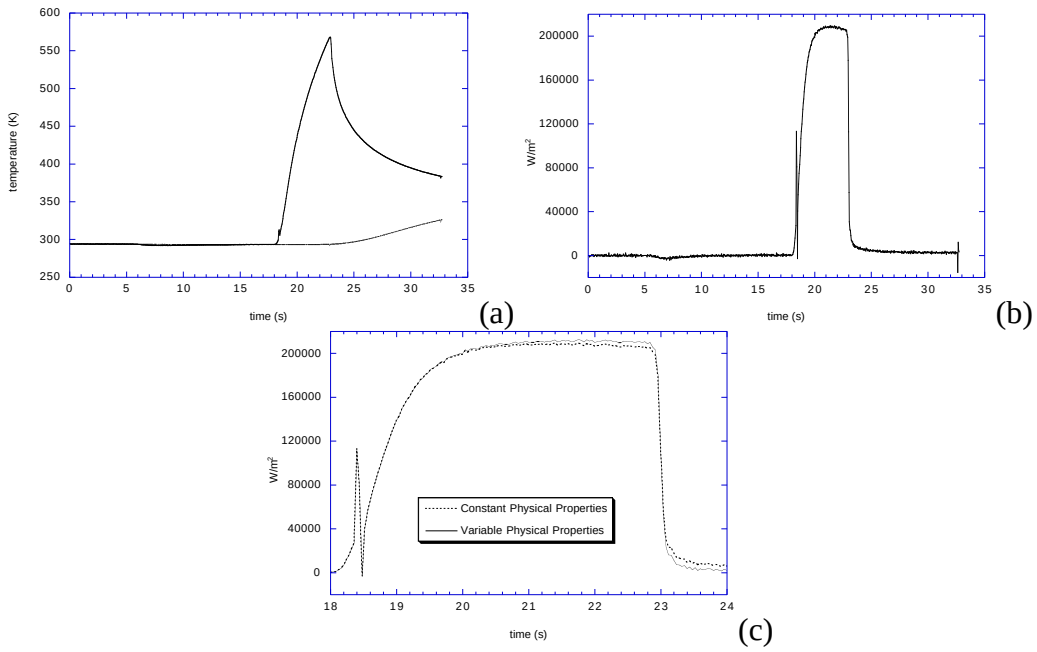


Fig. 11. Single layer thin film surface temperature signal and heat flux computation for test case 16